ELSEVIER

International Journal of Mass Spectrometry 215 (2002) 59–75

International Journal of Mass Spectrometry

www.elsevier.com/locate/ijms

Fourier transform ion cyclotron resonance detection: principles and experimental configurations

Alan G. Marshall*, Christopher L. Hendrickson

Center for Interdisciplinary Magnetic Resonance, National High Magnetic Field Laboratory, Florida State University, 1800 East Paul Dirac Drive, Tallahassee, FL 32310, USA

Received 8 August 2001; accepted 26 November 2001

Abstract

Fourier transform ion cyclotron resonance mass spectrometry is based on image current detection of coherently excited ion cyclotron motion. The detected signal magnitude and peak shape may be understood from idealized behavior: single ion, zero-pressure, spatially uniform magnetic field, three-dimensional axial quadrupolar electrostatic trapping potential, and spatially uniform resonant alternating electric field. In practice, deviation from any of the above conditions will shift, distort, split, and/or coalesce FT-ICR mass spectral peaks. Fortunately, such peak distortions may typically be avoided by appropriate experimental design and/or greatly minimized by internal frequency-to-*m*/*z* calibration. Various aspects of modern FT-ICR detection (hardware and software) are discussed. (Int J Mass Spectrom 215 (2002) 59–75) © 2002 Elsevier Science B.V. All rights reserved.

Keywords: Fourier transform; Ion cyclotron resonance; ICR; FTMS

1. Introduction

Broadband (e.g., ions of $200 < m/z < 1000$ detected simultaneously) Fourier transform ion cyclotron resonance mass spectrometry (FT-ICR MS) offers ultrahigh mass resolving power ($m/\Delta m_{50\%} > 300,000$ at 9.4 T, in which m is ion mass and $\Delta m_{50\%}$ is the mass spectral peak full width at half-maximum peak height), mass resolution ($m_2 - m_1 > 0.003$ Da), and mass accuracy (ppm rms), for complex mixtures containing compounds of up to several thousand different elemental compositions. That performance can improve by more than an order of magnitude for ions detected over a more limited *m*/*z* range. As explained below, the basis for that performance is that ions of a given *m*/*z* are detected according to their cyclotron *frequency*, and ions need to be confined for a sufficiently long period (∼1 s) to determine that frequency with high precision.

An FT-ICR MS experiment consists of a series of temporally separated events, typically: ion formation external to the detector, ion cooling/focusing/ accumulation, ion transmission to a Penning trap, mass-to-charge ratio (*m*/*z*)-selective ejection to select ions spanning a desired (*m*/*z*) range, dipolar excitation, dipolar analog detection with simultaneous analog-to-digital conversion and storage of the time-domain analog signal, apodization, fast Fourier transformation, magnitude computation, and frequency-to-*m*/*z*

* Corresponding author. Present address: Member, Department of Chemistry, Florida State University, Tallahassee, FL 32306 USA. E-mail: marshall@magnet.fsu.edu.

1387-3806/02/$20.00 © 2002 Elsevier Science B.V. All rights reserved.
PII S1387-3806(01)00588-7

conversion with respect to external or internal spectral peaks. Recent reviews describe the general features and variants of such experiments [1] as well as the milestones in historical evolution of each stage [2]. Here, we focus on principles and methods for detection of ion cyclotron rotation. Because ion cyclotron motion must be spatially coherent to be detectable, it is necessary to consider ion excitation as well. Because ions must be confined for extended detection periods, it is necessary to discuss means for ion trapping. Because the geometric requirements for excitation/detection and trapping are different, it is important to understand the tradeoffs in attempts to optimize both aspects in a single geometric configuration. Finally, we shall briefly discuss the effects of trap configuration, excitation mode, magnetic field strength, ion charge density, ion-neutral collisions, and digital data reduction on the appearance (position, shape, multiplicity, coalescence) of FT-ICR mass spectral peaks.

This discussion will be limited to image-charge detection, which has supplanted earlier detection based on charge collection ("omegatron" [3–6]) and power-absorption ("marginal oscillator" [7,8]) designs. We shall not describe single-ion detection of ion axial oscillation (see below) by a superconducting quantum interference device (SQUID). Such experiments have been used for ultraprecise atomic mass measurements [9], and to determine the (lack of) mass difference between the proton and antiproton [10]. However, because such experiments require liquid helium temperature, and report only a single m/z value at a time, they are not applicable to analytical mass spectrometry in which a wide range of m/z values must be covered quickly. Another non-FT detection method is axial ejection of the ions with time-of-flight mass analysis by single-ion counting [11]: that method is low-resolution but high-sensitivity.

2. Ion cyclotron motion

An ion of mass, m, and charge, q, moving in a spatially uniform magnetic field, B, rotates about the magnetic field direction as shown in Fig. 1. The "unperturbed" cyclotron (rotational) frequency, ω_c (SI units), is expressed in Eq. (1) [1].

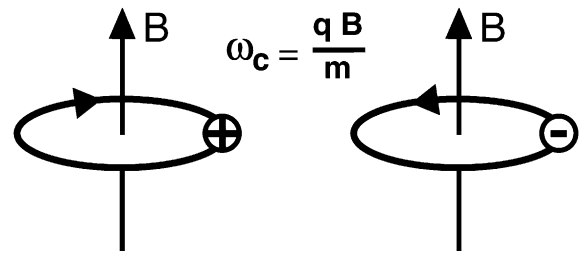

Fig. 1. Ion cyclotron motion. Ions rotate in a plane perpendicular to the direction of a spatially uniform magnetic field, B. Note that positive and negative ions orbit in opposite senses.

$$\omega_c = \frac{qB}{m} \tag{1a}$$

$$\nu_c = \frac{\omega_c}{2\pi} = \frac{1.535611 \times 10^7\, B}{m/z} \tag{1b}$$

in which ν_c is in hertz, B in tesla; m in microgram; z in multiples of elementary charge.

A notable feature of Eq. (1) is that *all* ions of a given mass-to-charge ratio, m/q, rotate at the *same* ICR frequency, *independent of velocity*. That property makes ICR especially amenable to mass spectrometry, because ion frequency is relatively insensitive to kinetic energy, so translational energy "focusing" is not essential for precise determination of m/z. Moreover, at a common static magnetic field value of 7.0 T (at which the corresponding proton NMR Larmor frequency is 300 MHz), ICR frequencies for ions of interest range from a few kHz to a few MHz, a particularly convenient range for commercially available broadband electronics.

3. Ion cyclotron excitation and detection

Treatment of resonant ion cyclotron dipolar excitation and detection begins from the idealized model of Fig. 2. The electric potential, $V(y)$, between two infinitely extended parallel conductor plates varies linearly with y. Thus, the corresponding electric field,

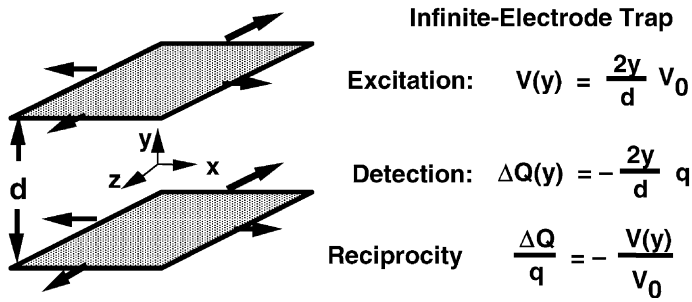

Fig. 2. Excitation voltage difference and detection induced charge difference in FT-ICR MS, demonstrated for two infinitely extended parallel flat electrodes located at $y = \pm d/2$ m away from the z-axis. If a potential, V_0, is applied to the upper electrode and $-V_0$ to the lower electrode, the potential, $V(y)$, anywhere between the electrodes is $2V_0y/d$. Conversely, if a point charge, q, is located between the same electrodes (in the absence of any applied voltage), then the difference, $\Delta Q(y)$, between the charge induced on the upper and lower electrodes is $-2\ q\ y/d$. It turns out that the relationship, $\Delta Q/q = -V/V_0$, is true (by the principle of "reciprocity", also known as Earnshaw's theorem [112]) for opposed electrodes of arbitrary shape. (Reproduced, with permission, from [1].)

$E(y) = -\partial[V(y)]/\partial y$, is constant anywhere between the two plates. Conversely, the difference in charge, $\Delta Q(y)$, induced by an ion of charge, q, at the same y-position, also varies linearly with y.

As for nuclear magnetic precession [12], ion cyclotron rotation is initially "incoherent," and does not by itself generate an observable electrical signal (for ICR, a net difference in the charge induced on two opposed parallel electrodes). At their instant of formation in (or injection into) the ion trap, ion cyclotron orbital *phases* are random—i.e., an ion may start its cyclotron motion at any point around either circle shown in Fig. 1. Thus, for an ensemble of ions, any charge induced on one detector plate will be balanced by an equal charge induced on the other detector plate (i.e., by an ion with opposite phase), so that the net difference in detected charge between the two plates is zero. Moreover, the cyclotron radius of thermal ions is too small to induce a detectable signal (i.e., proportional to y/d in Fig. 2), even if all ions had the same cyclotron phase.

FT-ICR detection is thus typically preceded by *excitation* produced by applying a spatially uniform electric field of amplitude, E_0, directed perpendicular to the magnetic field direction, and rotating at the cyclotron frequency of ions of a particular m/z value (i.e., "resonant"). During such excitation, the dimensions of the initial ion packet remain the same [13], and the packet accelerates along a spiral trajectory, as illustrated in Fig. 3 (left).

Following resonant irradiation of duration, T_{excite}, the post-excitation ion packet cyclotron radius, r (SI units), increases to

$$r = \frac{E_0 T_{\text{excite}}}{2B} \tag{2}$$

As described previously [1], a coherently orbiting ion packet induces a differential current between two opposed detection plates and may be modeled as a current source. The current amplitude is proportional to the number of spatially coherent orbiting ions. The receiver plates and wiring that connect the ion trap to the detection preamplifier have an inherent resistance and capacitance in parallel (Fig. 3) [14,15]. At typical ICR frequencies (>10 kHz) the signal-to-noise ratio is essentially independent of cyclotron frequency. However, at sufficiently low-frequency (<10 kHz), the signal is expected to vary directly with frequency [14,16]. Therefore, throughout most of the frequency range excited by a broadband waveform in a standard FT-ICR MS experiment, the detected signal-to-noise ratio reflects the relative current differential induced on the detection plates. Furthermore, the detection limit (namely, the minimum number, N, of ions that may be detected from an undamped signal in a single 1 s acquisition period to yield a S/N ratio of 3:1) may

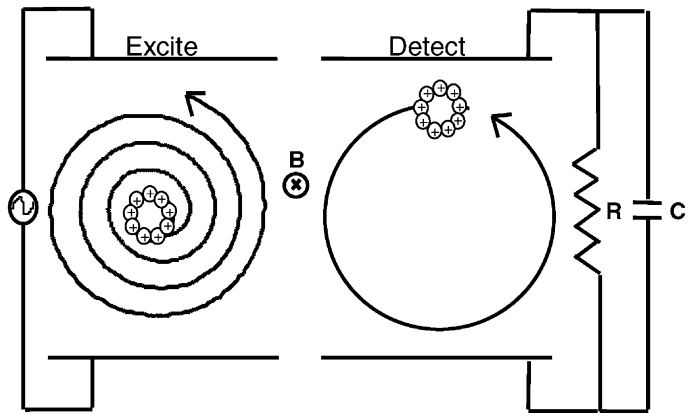

Fig. 3. Incoherent ion cyclotron orbital motion (left) is converted to coherent (and therefore detectable) motion (right) by application of an electric field that rotates in the same sense and at the ICR frequency of the ions of a given *m*/*z* value.

be calculated from [15]

$$N = \frac{CV_{\mathrm{d(p-p)}}}{qA_1(r)} \tag{3}$$

in which C is the capacitance of the detection circuit, $V_{\mathrm{d(p-p)}}$ is the peak-to-peak amplitude of the detected voltage (calibrated for a given spectrometer), and $A_1(r)$ is a trap configuration-dependent coefficient that is approximately proportional to r and may be determined graphically [17]. For example, for some typical operating parameters, namely, a detection circuit capacitance of 50 pF, $V_{\mathrm{d(p-p)}}$ of 3×10^{-7} V, and $A_1(r) = 0.5$ (i.e., the ion is excited to approximately half of its maximal cyclotron radius), an observed signal-to-noise ratio of 3:1 corresponds to a detection limit of ∼187 ions.

The ICR signal is proportional to the induced current, $\mathrm{d}\Delta Q/\mathrm{d}t = -2q(\mathrm{d}y/\mathrm{d}t)/d$ [14,15,18] (note that ICR signal is independent of magnetic field strength). Further, the induced current increases linearly with ion cyclotron radius (because the ion y-velocity component, $\mathrm{d}y/\mathrm{d}t$, increases linearly with radius), so the ICR signal increases *linearly* with ion cyclotron post-excitation radius. Linearity is important for several reasons. First, the ICR response at *any* frequency is proportional to the excitation spectral magnitude at that frequency, because the ICR signal varies linearly with ion cyclotron post-excitation radius (which depends linearly on the excitation voltage amplitude × duration product). Second, a Fourier transform of the time-domain ICR response gives the same "absorption" spectrum that is otherwise obtained by measuring power absorption while sweeping slowly across the *m*/*z* range [19]. In addition, the "superposition" principle implies that the signals from any number of ions of arbitrary *m*/*z* values simply add at the detector; thus, ions of a wide *m*/*z* range can be detected *simultaneously*. The two prior statements combine to constitute the "multichannel" advantage of pulsed excitation followed by Fourier transformation to yield a spectrum of N data points in $1/N$ the time it would take to scan the spectrum one channel at a time [19]. Finally, the detected signal increases linearly with ion charge, so that ICR is more sensitive for multiply-charged ions. For example, individual DNA ions of $\sim 10^8$ Da (each with ∼30,000 charges) have been detected by FT-ICR MS [20].

Although image current detection at room temperature is typically less sensitive than ion counting techniques characteristic of ion beam instruments, FT-ICR detection is non-destructive. Summing N repeated data acquisitions from the same sample of ions can thus potentially improve the signal-to-noise ratio of the accumulated data by a factor of $N^{1/2}$ [19]. Ion remeasurement was first achieved by allowing collisions to relax the ion cyclotron post-excitation orbital radius back to near-zero before the next excitation/detection cycle

[21]. Much more efficient (and faster) remeasurement was later performed by use of quadrupolar axialization to collapse the post-excitation ion cyclotron orbital radius to near-zero between acquisitions [22].

4. Penning trap

It is easy to show that mass resolving power, $m/\Delta m_{50\%}$, is equal to frequency resolving power, $\omega/\Delta\omega_{50\%}$, in ICR mass spectrometry [5,23]. Stated another way, $m/\Delta m_{50\%}$ can be thought of as the number of cyclotron orbits an ion makes during the data acquisition period [24]. Thus, it is desirable to confine ions for as long as possible after excitation in order to maximize mass resolving power. Although, cyclotron rotation inherently confines ions radially, it is necessary to apply an axial electric field gradient in order to keep ions from escaping axially (i.e., parallel to the magnetic field direction).

Fig. 4 shows isopotential surfaces for the three idealized electric potentials employed in FT-ICR MS [18]. First, the three-dimensional axial quadrupolar electrostatic "Penning trap" potential (Fig. 4, left) is optimal for axial confinement of ions. The advantages of such a trapping potential are: (a) the ion cyclotron motion remains independent of the other ion natural motions (namely, axial "trapping" oscillation along the magnetic field and rotational "magnetron" motion about the trap axis); and (b) the ion cyclotron frequency is independent of ion position within the trap [25]. Second, ion axialization [26,27] is optimally generated from the two-dimensional quadrupolar potential of Fig. 4, middle. Third, azimuthal (i.e., in a direction perpendicular to the magnetic field) dipolar excitation is optimally produced by applying an alternating voltage difference between two infinitely extended parallel flat conductors (Fig. 4, right), as noted in Fig. 2.

Any of the three potentials of Fig. 4 can in principle be generated from a set of conductive surfaces that follow the isopotential surfaces for a given symmetry. However, (a) it is clearly possible to achieve only one symmetry from one set of conductive surfaces, and (b) each idealized isopotential surface extends to infinity whereas the dimensions of any actual trap must be finite. Fortunately, any of several simple trap geometries (e.g., cubic or cylindrical, Fig. 5a and b) can approach all three of the desired potentials near the center of the trap. Deviations from linearity or quadrupolarity reduce the magnitude of the desired ICR signal (by factors that depend (non-linearly) on ion position within the trap and on the trap aspect (length-to-width) ratio [1,28]). Non-linearities also generate signals at frequencies obtained from sums and differences of the cyclotron, trapping, and magnetron frequencies [29].

A general approach to optimizing ICR trapping, excitation, and/or detection is to segment any or all of the electrodes as shown in Fig. 5(c–e). For example, the end-cap ("trapping") electrodes may be cylindrical in the "open" trap configuration of Fig. 5d, thereby

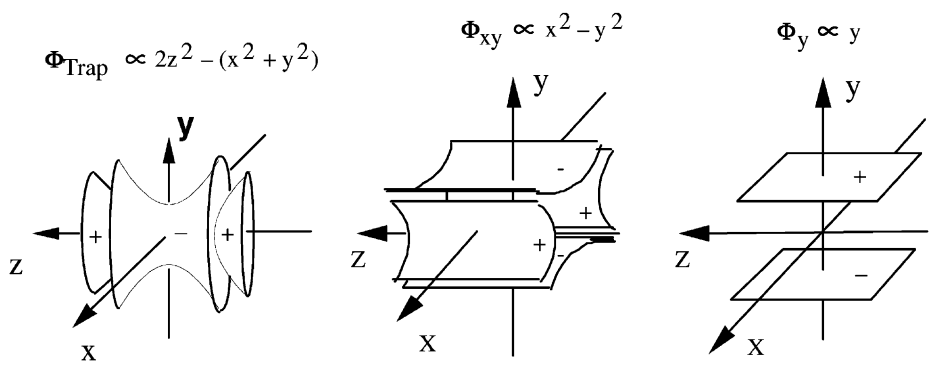

Fig. 4. Plot of isopotential surfaces for trapping (left), 2D quadrupolar (middle), and dipolar (right) potentials. The *z*-axis of the trap coincides with the direction of the applied magnetic field. (Reproduced, with permission, from [1].)

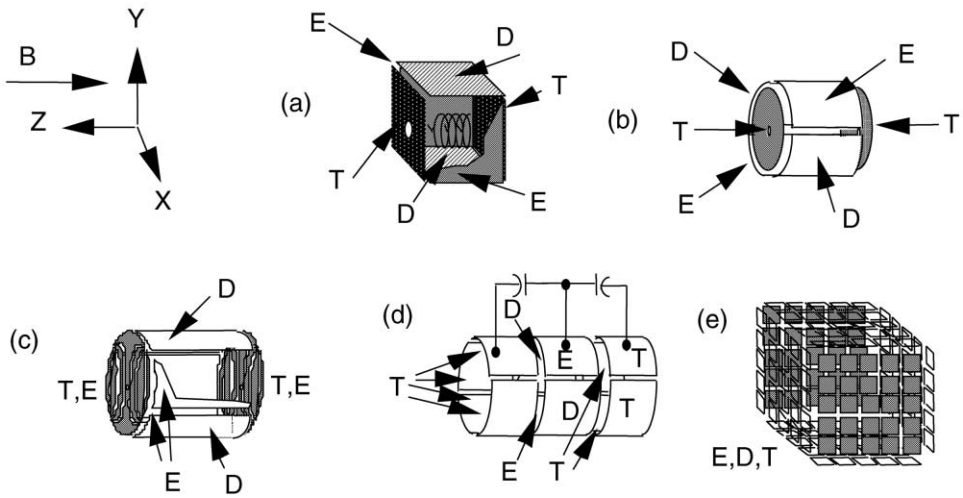

Fig. 5. ICR ion trap configurations. E = excitation; D = detection; T = end cap ("Trapping"). (a) cubic [16,113]; (b) cylindrical [45,114–116]; (c) end-caps segmented to linearize excitation potential ("infinity" trap) [117]; (d) open-ended, with capacitive rf coupling between the three sections [118–120] and (e) "matrix-shimmed" [18].

allowing for easier access of ions or photons or electrons into the trap. Capacitive coupling between the central and end-cap electrodes of the "open" cylindrical trap then effectively shorts the central and end-cap segments with respect to rf excitation, without affecting the static potential difference between the central and end-cap segments. The capacitively-coupled open trap thus provides for near-perfect dipolar rf electric field for ion cyclotron excitation. Similar linearization of the excitation field can be achieved by segmentation of the end-cap electrodes of a closed cylindrical trap (Fig. 5c). Ultimately, if *all* six sides of a cubic trap are segmented in grid fashion, and appropriate potentials applied to each individual grid element (Fig. 5e), then all three desired potentials of Fig. 4 can be approximated in a single geometric configuration.

The three-dimensional axial quadrupolar electrostatic trapping potential lowers the ICR frequency of Eq. (1) to the "reduced" cyclotron frequency, ω_+, given by

$$\omega_+ = \frac{\omega_c}{2} + \sqrt{\left(\frac{\omega_c}{2}\right)^2 - \frac{\omega_z^2}{2}} \tag{4a}$$

$$\omega_- = \frac{\omega_c}{2} - \sqrt{\left(\frac{\omega_c}{2}\right)^2 - \frac{\omega_z^2}{2}} \tag{4b}$$

in which the value of ω_c is given in Eq. (1a)

$$\omega_z = \sqrt{\frac{2qV_{trap}\alpha}{ma^2}} \tag{4c}$$

in which ω_z is the axial "trapping" oscillation frequency (SI units), V_{trap} is the potential applied to each end-cap electrode, a is a characteristic trap dimension (e.g., the length of one side of a cubic trap), and α is a parameter determined by the trap geometrical configuration (e.g., 2.77373 for a cubic trap) [1]. Note that

$$\omega_+ = \omega_c - \omega_- \tag{5}$$

Thus, because ω_- "magnetron" frequency is (except at very high m/z) independent of m/z, the shift in cyclotron frequency is also independent of m/z.

From Eq. (4), it is possible to derive [30]

$$\frac{m}{z} = \frac{A}{\omega_+} + \frac{B}{\omega_+^2} \tag{6}$$

One might expect Eqs. (4) and (5) to be valid only in the single-ion limit. Fortunately, it can be shown that a large ensemble of ions of a given m/z settles into an overall shape that generates a potential (acting on ions of other m/z values) of the same form (but opposite in

sign) to that of the axially quadratic trapping potential [31]. Thus, the form of Eq. (6) is preserved even in the presence of "space charge", and the constants, *A* and *B*, may be obtained by fitting to Eq. (6) a set of ICR mass spectral peak frequencies corresponding to ions of at least two known *m*/*z* values. Eq. (6) and its variants [32] are the standard frequency-to-*m*/*z* conversion ("calibration") expression for FT-ICR MS.

"Internal" calibration (i.e., calibrant ions are present along with analyte ions in the same sample) typically improves mass accuracy by a factor of 3–10 compared to "external" calibration (i.e., calibration is performed on a separate sample different from the analyte). External calibration works best when calibrant ions are excited to the same cyclotron radius as analyte ions and when the number of ions in the trap is the same for both experiments.

5. Ion–ion interactions

The effects of ion–ion interactions in a Penning trap are understood qualitatively, but not quantitatively. Experimentally, as the number of trapped ions increases, FT-ICR mass spectral peaks are observed to shift in frequency, broaden, and split or coalesce. Moreover, for a high population of trapped ions, the instantaneous ICR frequency can drift with time after excitation [33,34]. If ions are in constant supply, the best approach is to reduce the number of ions until all of the above effects become negligible. However, if the amount of sample is limited in amount or duration (as for on-line chromatography/mass spectrometry), it may not be possible to perform several independent measurements for each chromatographically separated component, and one must deal with the above "space charge" effects.

The equations of motion for two ions of the same *m*/*z* in a Penning trap can be solved analytically, and neither ion shifts the cyclotron frequency of the other [35]. Another Coulomb-mediated effect is that a packet of ions of the same *m*/*z* induces an "image" charge in the electrodes that surround the ions; however, the ICR frequency shift induced by that image-charge is typically negligible (e.g., $\sim 10^{-5}$ Hz per ion, at an ICR orbital radius equal to half the trap radius in a cubic trap [36]). The equations of ion motion also become solvable in the other extreme limit that the ion density is much higher ("plasma" conditions [37,38]) than in typical FT-ICR MS experiments.

Various authors have attempted to treat the problem of two packets of ions of different *m*/*z*. Because the problem cannot be solved analytically, it is necessary either to make various limiting assumptions about the packet shape and dynamics (e.g., point charge, ellipsoid of revolution, cylinder, dish, etc.) or solve Poisson's equation numerically for a limited number of ions [39]. To date, neither approach has been particularly helpful in quantitating FT-ICR mass spectral peak shape or Coulomb-induced ICR frequency shifts. However, some insight has been gained into the basis for experimentally observed peak coalescence [40] of ICR signals for ions of closely-spaced *m*/*z* values. Qualitatively, the difference in cyclotron velocity for two ions of the same charge, *q* and same cyclotron radius, *r*, is

$$v_2 - v_1 = (\omega_2 - \omega_1)r = qBr\left(\frac{1}{m_2} - \frac{1}{m_1}\right) \qquad (7)$$

Conversely, the velocity of a packet of ions moving in a plane perpendicular to an applied magnetic field, *B*, is *E*/*B*, in which *E* is the electric field produced by a second packet of ions of different *m*/*z*. Ion cyclotron resonances tend to coalesce when the common velocity due to the "$E \times B$" (i.e., ion–ion interaction) exceeds the difference in cyclotron velocities for the two ion packets. Of course, the electric field, *E*, is proportional to ion charge, *q*. The ratio, $(E/B)/qBr(1/m_2 - 1/m_1) = Em_1m_2/qB^2(m_1 - m_2)$, may thus, be thought of as a "coalescence" index—the bigger the ratio, the higher the coalescence tendency. This simplified argument explains the experimentally observed increased tendency for peak coalescence at higher ion mass, lower magnetic field strength, and closer ICR MS peak separation, as confirmed by more detailed theoretical analysis [41,42].

6. Heterodyne detection

When the first FT-ICR MS experiments were performed [43,44], analog-to-digital converters (ADCs) were not sufficiently fast, and buffer memory was not sufficiently large to sample and store a time-domain ICR signal spanning a wide *m*/*z* range (and thus, a wide range of ICR frequencies). It was therefore, necessary to employ "heterodyne" detection, in which the time-domain ICR signal is first multiplied ("mixed") with a single-frequency reference oscillator sinusoidal time-domain signal, thereby, generating signals at sum and difference frequencies of the reference and ICR signals (see Fig. 6). The mixing (multiplication) process in the time-domain corresponds to a convolution in frequency-domain—a spectrum of two ICR signals (S_1 at a frequency below the reference frequency, and S_2 at a frequency above the reference frequency) is thus convolved with the reference spectrum to produce components at the sum and difference frequencies [19]. The sum frequency signals are then suppressed by a low-pass filter, and the low-frequency band of difference frequencies can then be sampled and stored for subsequent discrete

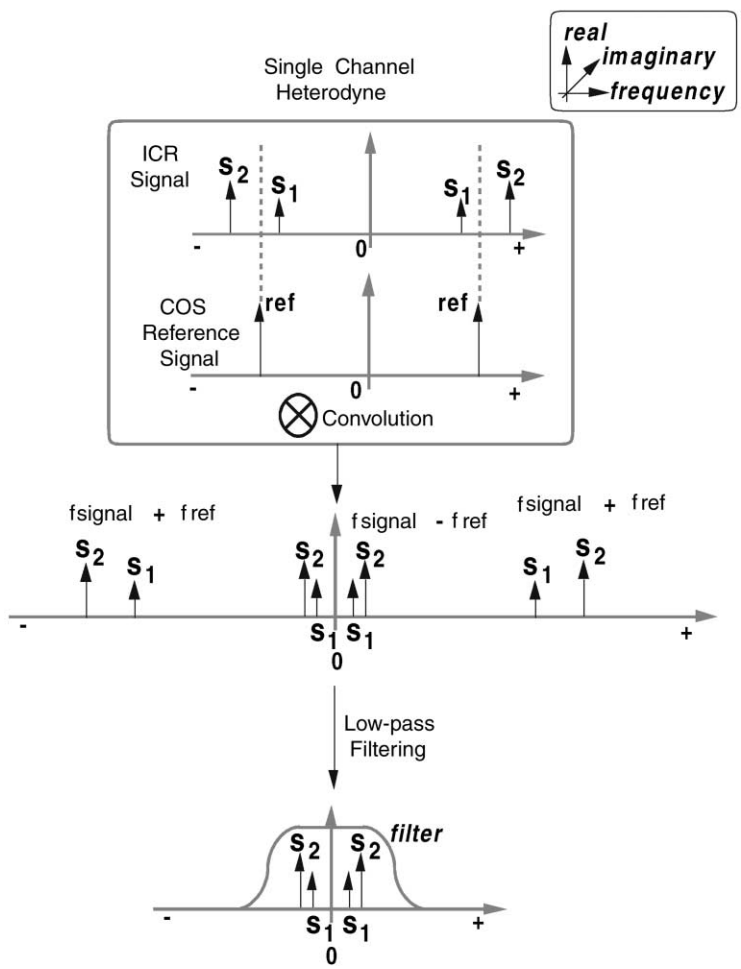

Fig. 6. Step-by-step procedure for heterodyne single-phase detection, represented in the frequency-domain. (Reproduced, with permission, from [49].)

Fourier transformation [45]. Now that commercial ADCs are available at e.g., 20 Msample/s, with buffer memory to 32 Mword, most FT-ICR mass spectra are now acquired in "direct" mode (i.e., direct sampling of the time-domain ICR analog signal.

Nevertheless, heterodyne-mode detection is still preferable to direct-mode detection when the highest mass resolution is needed over a restricted m/z range. For example, current world records for mass resolution are based on heterodyne detection: baseline resolution of two ~904 Da peptides separated by less than 0.0005 Da (i.e., less than the mass of a single electron) [46], and resolution of isotopic fine structure ($m/\Delta m_{50\%} > 5{,}000{,}000$) in a protein of ~16 kDa in mass [47].

7. Quadrature heterodyne detection

There are three problems with single-phase heterodyne detection. First, the inability to distinguish between ICR signals whose frequencies lie above or below the reference frequency results in spectral foldover (i.e., each signal on one side of the reference frequency also appears as its mirror image on the other side of the reference frequency). Thus, only half of the

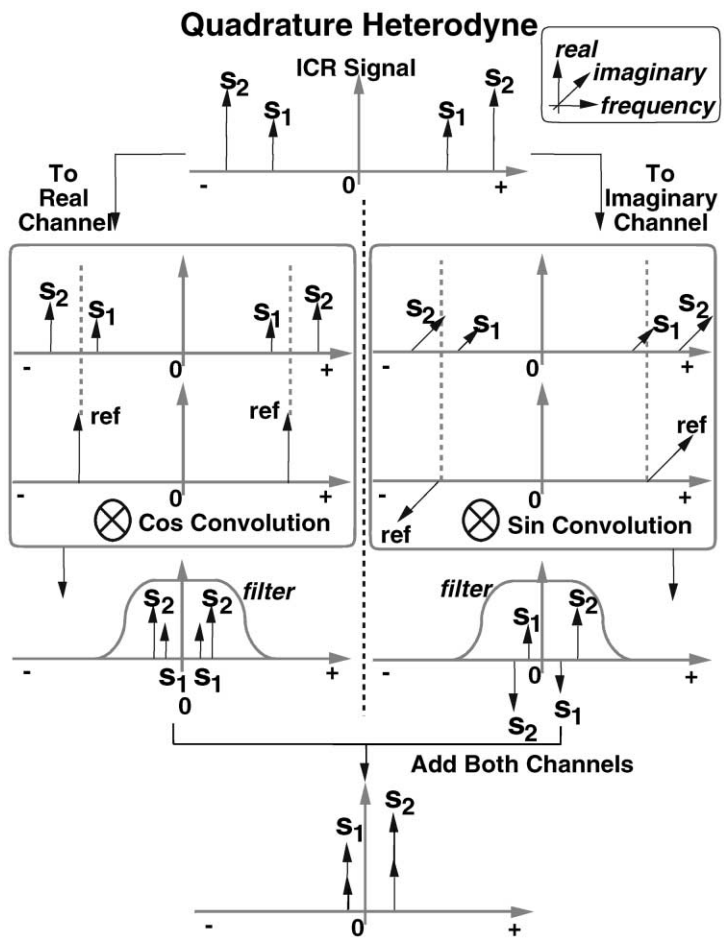

Fig. 7. Step-by-step procedure for quadrature heterodyne detection, represented in the frequency-domain. (Reproduced, with permission, from [49].)

available bandwidth is used, because the other half yields no new information. Second, it is not possible to distinguish between positive and negative ions, because linearly polarized dipolar irradiation may be analyzed as the sum of two counter-rotating components of the same frequency. One component will excite (or detect) positive ions and the other will excite (or detect) negative ions. Third, noise at frequencies (say) above the reference frequency is folded over into the other half of the spectrum, thereby increasing the rms noise by a factor of $2^{1/2}$, and reducing *S*/*N* ratio by the same factor, relative to direct-mode detection.

Foldover of signal and noise is eliminated in "quadrature" heterodyne detection, by distinguishing between signals whose frequencies lie above and below the reference frequency, as shown in Fig. 7. The ICR signal is divided into two equal components referred to as real and imaginary data. A cosine waveform is convolved with the real channel and a sine waveform is convolved with the imaginary channel. The reference waveforms (cosine and sine) have the same frequency but differ in phase by 90°. The data are treated with a low-pass filter, and the convolved real and imaginary data are summed to produce the final spectrum. The residual foldover peaks present in single-phase heterodyne detection are eliminated by that addition, because the foldover peaks have equal amplitude but opposite phase in the two channels (shown in Fig. 7). Adding the spectra from the two channels doubles the signal (thereby exactly compensating for halving the original signal when it was divided into two channels). The *S*/*N* ratio for quadrature heterodyne detection is thus, equal to that for direct detection, and exceeds that for single-phase heterodyne detection by a factor of $2^{1/2}$. Finally, although quadrature detection can be performed by analog [48] or digital [49] means, digital quadrature detection is preferable because (a) it eliminates noise from added analog oscillator, mixer, and filter components; (b) "image" peaks [19] resulting from unequal scaling of the two quadrature signals are eliminated; and (c) on-line digital filtering ensures that the filter bandwidth automatically matches the Nyquist bandwidth for optimal removal of noise without distorting the ion relative abundances.

8. Distinguishing positive and negative ions

Ordinarily, ions of only one charge sign are held in a Penning trap, because application of a positive (negative) electrostatic potential to the end-caps will trap only positive (negative) ions. However, it is possible to trap ions of both charge signs by applying an alternating potential to each of the end-caps [50–52], or by application of "nested" positive and negative static voltages [53–55]. In the former mode, ion axial motion is governed by a Mathieu equation, whose solution leads to a *z*-stability diagram for which optimal results are obtained at *z*-stability parameter, $q_z = (11.095)qV_{ac}/(md^2\Omega^2) \approx 0.5$, in which m/q is the ion mass-to-charge ratio, V_{ac} and Ω are the zero-to-peak amplitude and frequency of the applied alternating electric potential, and the numerical factor is for a cubic trap of edge length, *d*. The latter technique creates separate positive and negative potential wells inside the ICR cell volume.

Ion polarity may be distinguished based on opposite rotational phase by use of a different form of quadrature detection. In this case, the signal from one pair of opposed detection electrodes is stored as mathematically "real" and the signal from an orthogonal pair of detection electrodes is stored as mathematically "imaginary". Fourier transformation then produces a spectrum in which positive (negative) ions appear at positive (negative) frequency. Thus, it becomes easy to distinguish positive and negative ions of the same nominal mass in a single spectrum. For example, C_{60}^+ and C_{60}^- differ by only the mass of two electrons (∼0.001 Da) in single-phase detection, but differ by $(+720) - (-720) = 1440$ Da in quadrature detection [56]. We denote this experiment as "physical" quadrature (because the signals are detected on physically separate pairs of electrodes), whereas the "digital" quadrature of the preceding section is performed by software manipulation of the signal from a single pair of detection electrodes. (Conversely, by reciprocity

[57], ions of a single charge sign may be isolated by quadrature excitation [58] rather than quadrature detection.)

9. Ion-neutral collisions

The magnitude-mode FT-ICR mass spectral peak shape for an undamped time-domain signal (i.e., zero neutral pressure) is a "sinc-squared" function, with a series of decreasing-amplitude lobes on either side of the peak maximum [23] (see Fig. 8, top). The effect of ion-neutral collisions (reactive or non-reactive) is to damp the time-domain ICR signal. In the "high-pressure" limit that the ICR time-domain signal is collisionally damped essentially to zero during the acquisition period, the FT mass spectral peak shape is either Lorentzian (for the Langevin collision model) [59] (see Fig. 8, bottom), or a non-analytic function that is narrower at half-height but broader at the bottom than a Lorentzian (hard-sphere collision model) [60]. (Although, the Langevin model offers a good description for room-temperature ions, a hard-sphere collision model is much more appropriate for the much higher velocities of ions during FT-ICR data acquisition.) At intermediate collision frequency (e.g., collision lifetime of the order of the time-domain data acquisition period), the mass spectral line shape represents a convolution between the zero-pressure and high-pressure limiting line shapes [19,59] (Fig. 8, middle). In fact, ICR time-domain data are typically "windowed" (i.e., multiplied by any of several weight functions) to yield an "apodized" peak shape that is usually designed to narrow the otherwise broad skirts of the peak at the expense of slight increase in the width at half-maximum peak height [19].

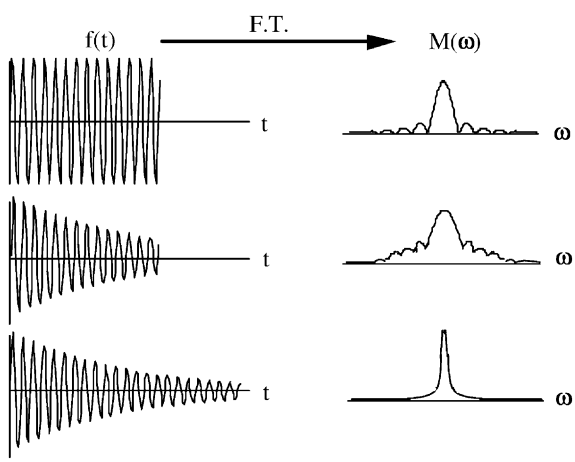

Fig. 8. Simulated time-domain ICR signals (left) and frequency-domain magnitude spectra (right) for low-pressure, $\tau \gg T_{acq}{}'_{n}$ (top), intermediate-pressure, $\tau \approx T_{acq}{}'_{n}$ (middle), and high-pressure, $\tau \ll T_{acq}{}'_{n}$ (bottom) limits. τ is the lifetime for ion-neutral collisions, $T_{acq}{}'_{n}$ is the data acquisition period, and the collision mechanism is assumed to be ion-induced dipole (Langevin [121]). (Reproduced, with permission, from [1].)

Ion-neutral collisions broaden and distort FT-ICR mass spectral peaks (but produce only a negligible frequency-shift). Thus, such collisions do not change the m/z values determined by frequency-to-m/z calibration [30,32], as long as the peaks are still well-resolved. However, even for well-resolved peaks, collisional broadening does reduce the precision of mass measurement, because that precision is proportional to the product of peak height and the square root of the number of data points per peak width [61]. Since, FT-ICR peak height varies inversely with peak width, $\Delta m_{50\%}$, precision varies as $(1/\Delta m_{50\%})^{1/2}$.

10. Fourier transform aspects of ICR excitation and detection

The most unique advantage of FT-ICR as a mass analyzer is that ion mass-to-charge ratio is experimentally manifested as a *frequency*. Because frequency can be measured more accurately than any other experimental parameter, ICR MS offers inherently higher resolution (and thus, higher mass accuracy) than any other type of mass measurement.

Various aspects of Fourier transform data reduction related to ICR peak shape and position have been discussed elsewhere: Nyquist sampling and foldover [62], fast Fourier transformation [63], zero-filling [64], "windowing" or apodization [19], deconvolution [65–67], oversampling [68], two-dimensional Hadamard [69] or Fourier [70] MS/MS, etc. Non-FT

methods for obtaining a frequency-domain (and thus mass-domain) spectrum from a digitized time-domain ICR signal include: the Hartley transform (a way of performing a Fourier transform on real-only data) [71,72], the Bayesian maximum entropy method (MEM) [73,74], linear prediction [75,76], and filter diagonalization [77]. However, FT data reduction is still overwhelmingly preferred, in part because non-FT methods typically require an order of magnitude more data storage; their computation time for an N-point time-domain data set typically scales as N^2 or N^3 (vs. $N \log_e N$ for the fast Fourier transform [63]); and they typically perform best when the number of spectral peaks is small and the peak shapes are uniform and known.

Finally, it is worth noting that Fourier transforms work backward (from frequency- to time-domain) as well as forward (from time- to frequency-domain). Thus, it is possible to specify a desired magnitude vs. frequency excitation spectrum, and apply an "inverse" Fourier transform to generate the corresponding time-domain waveform to be applied to the excitation electrodes of an ICR trapped-ion cell. Such "stored waveform inverse Fourier transform ("SWIFT") excitation [78] is now widely used in both FT-ICR [79] and Paul (quadrupole) [80,81] ion traps, for mass-selective excitation and ejection.

11. Effect of magnet strength and size on ICR detection

As noted in Section 2, the detected ICR signal *magnitude* is formally independent of applied magnetic field strength. Nevertheless, the *quality* of the detected signal improves dramatically with increasing magnetic field, B, for several other reasons [82]. (a) Mass resolving power (and mass measurement accuracy) in FT-ICR MS increase linearly with increasing B [23,59]. (b) Because ICR frequency increases linearly with B, the length of time needed to acquire data for a mass spectrum of a given resolving power varies inversely with B. Thus, data acquisition period-limited experiments, such as on-line LC/MS, are significantly enhanced at higher magnetic field strength. (c) The upper mass limit at which ions can be detected increases as B^2 [30]. (d) The maximum number of ions that can be confined without coalescence of their FT-ICR signals increases as B^2 [41], and the highest mass at which two packets of equally charged and equally abundant ions (independent of charge state) can be resolved to 1 Da varies as B [42]. (e) The maximum period that ions can be confined in a Penning trap varies as B^2. (f) The maximum post-excitation ion translational energy varies as B^2, for more efficient and/or extensive collisional fragmentation at higher magnetic field strength. (g) Ion cyclotron thermal (i.e., initial) radius varies inversely with B, so that an ion packet can be made more spatially coherent at high magnetic field strength. Finally, these various advantages may be exploited in combination, so as to produce even higher enhancement in a particular parameter: e.g., signal-to-noise ratio can improve by more than a factor of B^2 if mass resolving power is fixed at the same value as at lower magnetic field [83].

For a given spatial homogeneity, a larger magnet bore diameter, d, is also advantageous. (a) Dynamic range (i.e., ratio of most abundant to least abundant ions in the mass spectrum) increases as d^2. (b) Efficiency of removal of gases from the vacuum chamber increases as d^3. (c) A larger magnet bore facilitates introduction of multiple electrical feed-throughs as well as photon optics, and heating or cooling of the ion trap.

12. Harmonics and multiply segmented detector electrodes

Non-linearity in ICR time-domain signal magnitude as a function of ion cyclotron orbital radius leads to signals at (typically odd-numbered) multiples of the "fundamental" reduced ICR frequency of Eq. (4a) [84]. The non-linear component can provide an independent measure of the post-excitation ICR orbital radius [85]. However, harmonic signals are generally viewed as undesirable in FT-ICR MS,

because the fundamental ICR signal magnitude is reduced by the combined magnitudes of the harmonic signals; and harmonics increase the number of peaks in the mass spectrum and can interfere with identification of other fundamental (but low-magnitude) signals.

Nevertheless, more than a decade ago, it was proposed that FT-ICR mass spectral resolution could be improved by segmenting a Penning trap into multiple pairs of detection electrodes, and combining the signals from alternate pairs [86–88]. For n pairs of opposed electrodes, the detected ICR signal for ions of a given m/z would execute n cycles of oscillating signal, compared to just 1 cycle for the usual single pair of opposed detector electrodes. Thus, the ICR signal frequency would increase by a factor of n ("harmonic"). If the ICR signal duration were the same, then the FT-ICR spectral peak width would be the same, and mass resolving power would increase by a factor of n. Although, this general idea has been examined repeatedly since its inception [89–92], it has yet to be adopted for any chemical or biochemical applications. The main problems are: (a) it is difficult to configure a detector that will produce just a single multiple-harmonic signal—usually several harmonics are present, further complicating analysis; (b) the extent of improvement depends on the mechanism for damping of the time-domain ICR signal [90]; and (c) harmonic signal magnitude is small relative to that at the "fundamental" frequency unless the ICR orbital radius is very near to the cell maximum (at which non-linearities in electric and magnetic field lead to other problems) [93]. (Signals at other "combination" frequencies (e.g., sums and differences of integer multiples of ω_+, ω_c, and ω_-, can result from non-linearities in the electric fields applied to the ion trap [29]. These signals may be enhanced by appropriate detection schemes [94].)

At this point, the reader might wonder how one can distinguish signals at harmonic frequencies (i.e., $n\,\omega_+$, in which $n = 2, 3, 4, \ldots$) for a singly-charged ion from the fundamental cyclotron frequency (ω_+) for multiply-charged dimers of the same ion (e.g., $[2M + 2H]^{2+}$ vs. $[M + H]^+$ or $[2M + 2e]^{2-}$ vs. $[M + e]^-$). One way is to measure the m/z separation between the quasimolecular ion whose carbon atoms are all ^{12}C and the same species in which one of the carbons is ^{13}C—the m/z separation will be $1/z$ [95]. A second way is to change the trapping potential: multiply-charged and singly-charged ions will exhibit the same frequency shift, whereas the signal at a harmonic frequency will shift by n times as much as the signal at the fundamental frequency. The latter method was used in the first demonstration of a fullerene gas-phase dianion [96].

13. New developments and directions

With current (year 2002) FT-ICR MS detector technology, it is already possible to resolve and identify up to thousands of components of a complex mixture, often without prior wet chemical separation, thereby potentially changing the whole approach to dealing with chemical and biological complexity. More than 360 FT-ICR mass spectrometers have been installed worldwide. We now consider some projected future improvements.

13.1. Magnets

Given the multiple independent advantages offered by higher magnetic field, an obvious direction for future ICR technology is toward higher-field magnets. Superconducting magnets up to 11.5 T [97] are already in use for ICR, with at least one 15 T system scheduled for installation in 2002 at NHMFL. FT-NMR superconducting magnets up to 21.1 T (900 MHz for ^1H NMR) systems are already commercially available. FT-ICR MS has been performed at 20 T [98] and 25 T [99] with resistive magnets, and even better performance can be anticipated from a hybrid magnet whose superconducting and resistive coils are connected in series (so that the high inductance of the superconducting magnet will limit temporal fluctuations in the low-inductance resistive coil). There are no technical barriers to such a hybrid magnet up to at least 27 T with 110 mm bore diameter.

13.2. FT data reduction

FT-ICR mass spectra are currently reported as "magnitude"-mode, i.e., the square root of the sum of the squares of the "real" and "imaginary" spectra that result from FT of a time-domain signal. From the outset, it was recognized that significantly higher mass resolving power (factor ranging from $\sim\sqrt{3}$ (Lorentzian peak shape) to 2 (sinc peak shape) [59] may be realized by appropriate "phasing" (i.e., linear combination of the raw "real" and "imaginary" spectra to yield an "absorption"-mode spectrum [100]. Resolving power improves even more near the base of each peak. Moreover, access to absorption-mode display makes it possible to discriminate between different collisional line-broadening mechanisms [101]. There have been a few reports of absorption-mode FT-ICR mass spectra [101,102], and the improvement in mass resolving power was clearly demonstrated.

However, the two big problems have been to correct for the (non-linear) phase variation introduced by the broadband (e.g., frequency-sweep) excitation itself and the time delay between the end of the excitation event and the beginning of the detection event (to provide for "ringdown" of the excitation signal at the detector electrodes). A time delay longer than one-half of one "dwell" period (i.e., the interval between acquisition of successive time-domain data points) introduces uncorrectable baseline modulation into the final FT spectrum [19]. Deconvolution of the non-linear magnitude vs. frequency spectrum of the excitation signal has been demonstrated theoretically for frequency-sweep excitation [65]. However, such deconvolution requires that excitation and detection are simultaneous. Simultaneous excitation and (non-FT) single-frequency detection was introduced in 1971, but never followed up [103]. Simultaneous excitation/narrow-band detection was explored briefly in the 1970's [104] (by analogy to "correlation" NMR [105]), but was soon abandoned (in both NMR and ICR) because the experiment was much slower (and more difficult to "tune") than the FT experiment. Recently, simultaneous broadband excitation/detection has been achieved, by careful tuning of a small air-gap capacitor to null the excitation signal at the detector electrodes [106] It should be possible to apply that experiment to phase a broadband FT-ICR mass spectrum, to yield significant improvement in mass resolution.

The combination of digitizers of higher precision (>20 bit/word), speed (>10 MHz), and storage (>16 Mwords) with high-speed (1 Mword FFT in <0.4 s) desktop computers means that it is increasingly possible to acquire most FT-ICR MS data in direct-mode, without the need for heterodyning. For example, we have recently demonstrated an average mass resolving power of >300,000 over a range, $200 < m/z < 1000$, at 9.4 T, based on direct-mode detection (4 Mword). That approach becomes increasingly desirable for LC/MS applications, in which all of the ICR data must be acquired during the passage (a few seconds) of the LC peak into the mass spectrometer.

13.3. FT-ICR operating modes

The evolution of FT-ICR MS shares many features in common with the (generally prior) development of FT nuclear magnetic resonance spectroscopy [12,107]. In fact, there are deep homologies that connect virtually every kind of FT-NMR experiment with an analogous one in FT-ICR MS, ranging from "spin-locking" [108] ("ion-locking" [109]) to two-dimensional NOESY (NMR) or SWIM (ICR) for identifying coupled spins (NMR [110]) or coupled ion-molecule reactions (ICR [70]). However, one FT-NMR experiment that has not yet been applied to FT-ICR is time-shared excitation/detection, introduced in NMR as "tailored" excitation [111]. Like SWIFT excitation, tailored excitation begins from a time-domain waveform generated by inverse FT of the desired frequency-domain excitation spectrum. However, that waveform is then turned on and off as it proceeds, so that detection may take place during the intervals that the excitation is turned off. The excitation envelope may consist of pulses of equal duration and varying amplitude or (electronically simpler) of constant amplitude and varying duration. In this way,

one achieves essentially simultaneous excitation and detection, but without having to "null" the excitation by a large factor at the detector. Tailored excitation thus, offers an alternate route to generation of the absorption-mode spectrum discussed in Section 13.2.

Acknowledgements

This work was supported by NSF (CHE-99-09502), NIH (GM/RR-31683), Florida State University, and the National High Magnetic Field Laboratory in Tallahassee, FL.

References

[1] A.G. Marshall, C.L. Hendrickson, G.S. Jackson, Mass Spectrom. Rev. 17 (1998) 1–35.
[2] A.G. Marshall, Int. J. Mass Spectrom. 200 (2000) 331–336.
[3] H. Sommer, H.A. Thomas, J.A. Hipple, Phys. Rev. 76 (1949) 1877.
[4] H. Sommer, H.A. Thomas, Phys. Rev. 78 (1950) 806.
[5] H. Sommer, H.A. Thomas, J.A. Hipple, Phys. Rev. 82 (1951) 697–702.
[6] P.V. Ameri, H.R. Krouse, H. Fichtner, Rev. Sci. Instrum. 72 (2001) 2036–2042.
[7] N.I. Leont'ev, Instrum. Techn. (in English) 2 (1960) 275–281.
[8] D. Wobschall, Rev. Sci. Instrum. 36 (1965) 466.
[9] F. DiFillip, V. Natarajan, M. Bradley, F. Palmer, D.E. Pritchard, Phys. Scripta T59 (1995) 144–154.
[10] G. Gabrielse, X. Fei, L.A. Orozco, R.L. Tjoelker, J. Haas, H. Kalinowsky, T.A. Trainor, W. Kells, Phys. Rev. Lett. 65 (1990) 1317–1320.
[11] G. Bollen, H.-J. Kluge, M. Konig, T. Otto, H. Stolzenberg, R.B. Moore, G. Rouleau, G. Audi, Phys. Rev. C 46 (1992) R2140–R2143.
[12] A.G. Marshall, Acc. Chem. Res. 9 (1996) 307–316.
[13] M. Wang, A.G. Marshall, Int. J. Mass Spectrom. Ion Proc. 100 (1990) 323–346.
[14] M.B. Comisarow, J. Chem. Phys. 69 (1978) 4097–4104.
[15] P.A. Limbach, P.B. Grosshans, A.G. Marshall, Anal. Chem. 65 (1993) 135–140.
[16] M.B. Comisarow, Int. J. Mass Spectrom. Ion Phys. 37 (1981) 251–257.
[17] P.B. Grosshans, A.G. Marshall, Int. J. Mass Spectrom. Ion Proc. 100 (1990) 347–379.
[18] S. Guan, A.G. Marshall, Int. J. Mass Spectrom. Ion Proc. 146/147 (1995) 261–296.
[19] A.G. Marshall, F.R. Verdun, Fourier Transforms in NMR, Optical, and Mass Spectrometry: A User's Handbook, Elsevier, Amsterdam, 1990.
[20] R. Chen, X. Cheng, D.W. Mitchell, S.A. Hofstadler, Q. Wu, A.L. Rockwood, M.G. Sherman, R.D. Smith, Anal. Chem. 67 (1995) 1159–1163.
[21] E.R. Williams, K.D. Henry, F.W. McLafferty, J. Am. Chem. Soc. 112 (1990) 6157–6162.
[22] J.P. Speir, G.S. Gorman, C.C. Pitsenberger, C.A. Turner, P.P. Wang, I.J. Amster, Anal. Chem. 65 (1993) 1746–1752.
[23] M.B. Comisarow, A.G. Marshall, J. Chem. Phys. 64 (1976) 110–119.
[24] A.G. Marshall, C.L. Hendrickson, Rapid Commun. Mass Spectrom. 15 (2001) 232–235.
[25] L.S. Brown, G. Gabrielse, Rev. Mod. Phys. 58 (1986) 233–311.
[26] G. Savard, S. Becker, G. Bollen, H.-J. Kluge, R.B. Moore, L. Schweikhard, H. Stolzenberg, U. Wiess, Phys. Lett. A 158 (1991) 247–252.
[27] L. Schweikhard, S. Guan, A.G. Marshall, Int. J. Mass Spectrom. Ion Proc. 120 (1992) 71–83.
[28] G. Jackson, J.D. Canterbury, S. Guan, A.G. Marshall, J. Am. Soc. Mass Spectrom. 8 (1997) 283–293.
[29] A.G. Marshall, P.B. Grosshans, Anal. Chem. 63 (1991) 215A–229A.
[30] E.B. Ledford Jr., D.L. Rempel, M.L. Gross, Anal. Chem. 56 (1984) 2744–2748.
[31] J.B. Jeffries, S.E. Barlow, G.H. Dunn, Int. J. Mass Spectrom. Ion Proc. 54 (1983) 169–187.
[32] S.D.-H. Shi, J.J. Drader, M.A. Freitas, C.L. Hendrickson, A.G. Marshall, Int. J. Mass Spectrom. 195/196 (2000) 591–598.
[33] J.E. Bruce, G.A. Anderson, S.A. Hofstadler, B.E. Winger, R.D. Smith, Rapid Commun. Mass Spectrom. 7 (1993) 700–703.
[34] S. Guan, M.C. Wahl, A.G. Marshall, Anal. Chem. 65 (1993) 3647–3653.
[35] C. Gerz, D. Wilsdorf, G. Werth, Nuc. Instrum. Meth. Phy. Res. B47 (1990) 453–461.
[36] X. Xiang, P.B. Grosshans, A.G. Marshall, Int. J. Mass Spectrom. Ion Proc. 125 (1993) 33–43.
[37] T.M. O'Neil, Phys. Scripta T59 (1995) 341–351.
[38] A.J. Peurrung, R.T. Kouzes, S.E. Barlow, Int. J. Mass Spectrom. Ion Proc. 157/158 (1996) 39–83.
[39] D.W. Mitchell, J. Am. Soc. Mass Spectrom. 10 (1999) 136–152.
[40] Y. Naito, M. Inoue, J. Mass Spectrom. Soc. Jpn. 42 (1994) 1–9.
[41] D.W. Mitchell, R.D. Smith, Phys. Rev. E 52 (1995) 4366–4386.
[42] D.W. Mitchell, R.D. Smith, J. Mass Spectrom. 31 (1996) 771–790.
[43] M.B. Comisarow, A.G. Marshall, Chem. Phys. Lett. 25 (1974) 282–283.
[44] M.B. Comisarow, A.G. Marshall, Chem. Phys. Lett. 26 (1974) 489–490.
[45] M.B. Comisarow, A.G. Marshall, US Patent (1976).
[46] F. He, C.L. Hendrickson, A.G. Marshall, Anal. Chem. 73 (2001) 647–650.

[47] S.D.-H. Shi, C.L. Hendrickson, A.G. Marshall, Proc. Natl. Acad. Sci. U.S.A. 95 (1998) 11532–11537.
[48] F.R. Verdun, S.L. Mullen, T.L. Ricca, A.G. Marshall, FACSS XIV, Detroit, MI, 1987 (Abstract #41).
[49] J.J. Drader, S.D.-H. Shi, G.T. Blakney, C.L. Hendrickson, D.A. Laude, A.G. Marshall, Anal. Chem. 71 (1999) 4758–4763.
[50] M.V. Gorshkov, S. Guan, A.G. Marshall, Rapid Commun. Mass Spectrom. 6 (1992) 166–172.
[51] C.B. Jacoby, C.L. Holliman, D.L. Rempel, M.L. Gross, J. Am. Soc. Mass Spectrom. 4 (1993) 186–189.
[52] V. Frankevich, R. Zenobi, Int. J. Mass Spectrom. Ion Proc. 207 (2001) 57–67.
[53] G. Gabrielse, S.L. Rolston, L. Haarsma, W. Kells, Phys. Lett. A (1988) 38–42.
[54] Y. Wang, K.-P. Wanczek, Rev. Sci. Instrum. 64 (1993) 883–889.
[55] V.H. Vartanian, D.A. Laude, Org. Mass Spectrom. 29 (1994) 692–694.
[56] J.J. Drader, L. Schweikhard, S.D.-H. Shi, C.L. Hendrickson, A.G. Marshall, in: Proceedings of the 50th Pittsburgh Conference on Analytical Chemistry and Applied Spectroscopy, Orlando, FL, 1999 (Abstract #2065P).
[57] W. Shockley, J. Appl. Phys. 9 (1938) 635.
[58] L. Schweikhard, A.G. Marshall, J. Am. Soc. Mass Spectrom. 4 (1993) 433–452.
[59] A.G. Marshall, M.B. Comisarow, G. Parisod, J. Chem. Phys. 71 (1979) 4434–4444.
[60] S. Guan, G.-Z. Li, A.G. Marshall, Int. J. Mass Spectrom. Ion Proc. 167/168 (1998) 185–194.
[61] L. Chen, C.E. Cottrell, A.G. Marshall, Chemometr. Intell. Lab. Syst. 1 (1986) 51–58.
[62] M. Wang, A.G. Marshall, Anal. Chem. 60 (1988) 341–344.
[63] J.W. Cooley, J.W. Tukey, Math. Comput. 19 (1965) 297.
[64] M.B. Comisarow, J. Melka, Anal. Chem. 51 (1979) 2198–2203.
[65] A.G. Marshall, Chem. Phys. Lett. 63 (1979) 515–518.
[66] A.G. Marshall, D.C. Roe, J. Chem. Phys. 73 (1980) 1581–1590.
[67] Z. Zhang, S. Guan, A.G. Marshall, J. Am. Soc. Mass Spectrom. 8 (1997) 659–670.
[68] G.M. Alber, A.G. Marshall, Appl. Spectrosc. 44 (1990) 1111–1116.
[69] E.R. Williams, S.Y. Loh, F.W. McLafferty, R.B. Cody, Anal. Chem. 62 (1990) 698–703.
[70] C.W. Ross III, S. Guan, P.B. Grosshans, T.L. Ricca, A.G. Marshall, J. Am. Chem. Soc. 115 (1993) 7854–7861.
[71] C.P. Williams, A.G. Marshall, Anal. Chem. 61 (1989) 428–431.
[72] C.P. Williams, A.G. Marshall, Anal. Chem. 64 (1992) 916–923.
[73] J.E. Meier, A.G. Marshall, Anal. Chem. 62 (1990) 201–208.
[74] J.E. Meier, A.G. Marshall, Anal. Chem. 63 (1991) 551–560.
[75] J.F. Loo, M.D. Krahling, T.C. Farrar, Rapid Commun. Mass Spectrom. 4 (1990) 297–299.
[76] S. Guan, A.G. Marshall, Anal. Chem. 69 (1997) 1156–1162.
[77] P.B. O'Connor, V. Mandelshtam, M.R.T., in: Proceedings of the 47th American Society Mass Spectrometry Conference on Mass Spectrometry and Allied Topics, Am. Soc. Mass Spectrom., Dallas, TX, 1999, ThPB017.
[78] A.G. Marshall, T.-C.L. Wang, T.L. Ricca, J. Am. Chem. Soc. 107 (1985) 7893–7897.
[79] S. Guan, A.G. Marshall, Int. J. Mass Spectrom. Ion Proc. 157/158 (1996) 5–37.
[80] S. Guan, A.G. Marshall, Anal. Chem. 65 (1993) 1288–1294.
[81] R.K. Julian Jr., R.G. Cooks, Anal. Chem. 65 (1993) 1827–1833.
[82] A.G. Marshall, S. Guan, Rapid Commun. Mass Spectrom. 10 (1996) 1819–1823.
[83] M.W. Senko, C.L. Hendrickson, L. Pasa-Tolic, J.A. Marto, F.M. White, S. Guan, A.G. Marshall, Rapid Commun. Mass Spectrom. 10 (1996) 1824–1828.
[84] P.B. Grosshans, P.J. Shields, A.G. Marshall, J. Am. Chem. Soc. 112 (1990) 1275–1277.
[85] P.B. Grosshans, A.G. Marshall, Int. J. Mass Spectrom. Ion Proc. 115 (1992) 1–19.
[86] E.N. Nikolaev, M.V. Gorshkov, A.V. Mordehai, V.L. Talrose, USSR Patent (1987).
[87] Y.P. Pan, D.P. Ridge, J. Wronka, A.L. Rockwood, Rapid Commun. Mass Spectrom. 1 (1987) 121.
[88] Y.P. Pan, D.P. Ridge, A.L. Rockwood, Int. J. Mass Spectrom. Ion Proc. 84 (1988) 293.
[89] P. Kofel, M. Allemann, H. Kellerhals, K.P. Wanczek, in: P. Longevialle (Ed.), Advances in Mass Spectrometry, Heyden and Son., Ltd., London, 1989, 676–677.
[90] P.B. Grosshans, A.G. Marshall, Int. J. Mass Spectrom. Ion Proc. 107 (1991) 49–81.
[91] P.A. Limbach, P.B. Grosshans, A.G. Marshall, Int. J. Mass Spectrom. Ion Proc. 123 (1993) 41–47.
[92] M. Knobeler, K.P. Wanczek, Int. J. Mass Spectrom. Ion Proc. 125 (1993) 127.
[93] E.N. Nikolaev, M.V. Gorshkov, A.V. Mordehai, V.L. Talrose, Rapid Commun. Mass Spectrom. 4 (1990) 144–146.
[94] L. Schweikhard, M. Lindinger, H.-J. Kluge, Int. J. Mass Spectrom. Ion Proc. 98 (1990) 25–33.
[95] K.D. Henry, F.W. McLafferty, Org. Mass Spectrom. 25 (1990) 490–492.
[96] P.A. Limbach, L. Schweikhard, K.A. Cowen, M.T. McDermott, A.G. Marshall, J.V. Coe, J. Am. Chem. Soc. 113 (1991) 6795–6798.
[97] M.V. Gorshkov, L. Pasa-Tolic, H.R. Udseth, G.A. Anderson, B.M. Huang, J.E. Bruce, P.D.C., S.A. Hofstadler, L. Tang, L.-Z. Chen, J.A. Willett, A.L. Rockwood, M.S. Sherman, R.D. Smith, J. Am. Soc. Mass Spectrom. 9 (1998) 692–700.
[98] C.L. Hendrickson, J.J. Drader, D.A. Laude Jr., S. Guan, A.G. Marshall, Rapid Commun. Mass Spectrom. 10 (1996) 1829–1832.
[99] S.D.-H. Shi, J.J. Drader, C.L. Hendrickson, A.G. Marshall, J. Am. Soc. Mass Spectrom. 10 (1999) 265–268.
[100] M.B. Comisarow, A.G. Marshall, Can. J. Chem. 52 (1974) 1997–1999.
[101] B.A. Vining, R.E. Bossio, A.G. Marshall, Anal. Chem. 71 (1999) 460–467.

[102] E.C. Craig, I. Santos, A.G. Marshall, Rapid Commun. Mass Spectrom. 1 (1987) 33–37.
[103] P.P. Genequand, Z. Angew. Math. Phys. 22 (1971) 951–975.
[104] R.T. Hunter, R.T. McIver Jr., Chem. Phys. Lett. 49 (1977) 577.
[105] J. Dadok, R.F. Sprecher, J. Magn. Reson. 13 (1974) 243.
[106] S.C. Beu, in: Proceedings of the 46th American Society of Mass Spectrometry Conference on Mass Spectrometry and Allied Topics, Am. Soc. Mass Spectrom., Orlando, FL, 1998, p. 502.
[107] A.G. Marshall, Acc. Chem. Res. 18 (1985) 316–322.
[108] I. Solomon, Compt. Rend. Acad. Sci. Paris 248 (1959) 92–94.
[109] R. Chen, A.G. Marshall, M. Wang, Chem. Phys. Lett. 181 (1991) 168–174.
[110] G. Bodenhausen, R.R. Ernst, J. Am. Chem. Soc. 104 (1982) 1304–1309.
[111] B.L. Tomlinson, H.D.W. Hill, J. Chem. Phys. 59 (1973) 1775–1784.
[112] W.T. Scott, Am. J. Phys. 27 (1959) 418–419.
[113] M.B. Comisarow, Adv. Mass Spectrom. 8 (1980) 1698–1706.
[114] S.H. Lee, K.-P. Wanczek, H. Hartmann, Adv. Mass Spectrom. 8B (1980) 1645–1649.
[115] P. Kofel, M. Allemann, H. Kellerhals, K.-P. Wanczek, Int. J. Mass Spectrom. Ion Proc. 74 (1986) 1–12.
[116] J.L. Elkind, F.D. Weiss, J.M. Alford, R.T. Laaksonen, R.E. Smalley, J. Chem. Phys. 88 (1988) 5215–5224.
[117] P. Caravatti, M. Allemann, Org. Mass Spectrom. 26 (1991) 514–518.
[118] G. Gabrielse, L. Haarsma, S.L. Rolston, Int. J. Mass Spectrom. Ion Proc. 88 (1989) 319–332.
[119] S.C. Beu, D.A. Laude Jr., Anal. Chem. 64 (1992) 177–180.
[120] S.C. Beu, D.A. Laude Jr., Int. J. Mass Spectrom. Ion Proc. 112 (1992) 215–230.
[121] P. Langevin, Ann. Chim. Phys. 5 (1905) 245.